FACIES AND SEDIMENTOLOGY OF THE SANTA MARIA FORMATION

Lower marine unit

This unit is dominated by black sandstones with minor interbedded layers of clay, peat, paleosol, and locally fine conglomerate. The black sandstones are medium to coarse, occasionally showing grading to fine conglomerate. They consist mainly of volcanic lithic components (85 to 90%), minor quartz (3%), feldspars and other minerals (7 to 12%), occasionally retransported volcanic tuffs and small shell fragments (Figs. DR2). Within these deposits there are zones of intense vertical bioturbation and highly contorted limonitic layers. The sandstone beds are not laterally continuous and thin-out rapidly (Fig. DR3). The main sedimentary structures found in the black sandstone are coarse cross bedding in individual beds that can reach a thickness of 10 m, wavy flaser bedding, and fine inclined and parallel lamination. Locally, individual successive rhythmic upward-coarsening sequences of medium to pebbly sand and fine conglomerate characterize this unit. Grain-size distribution curves from this unit resemble curves obtained from present-day shore depositional environments of the island (Fig. DR1).

The interbeded layers consist of: (1) grey clay with 10 to 30 cm mean thickness (but locally up to 1.5 m) that typically contains charcoal and occasionally wood; (2) dark-brown clay-rich paleosols, ranging from 10 cm to ~1 m in thickness and that also contain charcoal; (3) black peat, about 1-m thick containing wood; and (4) very rounded conglomerates with metamorphic and occasional volcanic clasts, 2 to 3 cm in diameter but that can reach 30 cm. These bed usually form lenses reaching a lateral continuity of 50 m.

The volcanic-rich black sand derive from basaltic lavas of the Antuco volcano in the Main Cordillera (Fig. 1B). During Pleistocene time, opening of Lake Laja, adjacent to the volcano, caused a catastrophic megaflood that formed fans in the Central Depression composed of volcanic-derived material (Vergara and Katsui, 1969), which have been since transported to the coast by the Laja, Itata, and Bío-Bío rivers (Fig. 1B). These black sands are unique and thus found in the vicinity of these rivers, suggesting that the volcanic-rich sandstone and associated metamorphic and volcanic gravels were transported to the continental shelf by the Bío-Bío river when sea level was lower, and subsequently reworked in a near-shore marine environment.

Upper eolian unit

This unit consists of homogeneous very well sorted brownish sandstone. The medium size sandstone are composed of volcanic lithic components (50 to 65%), feldspars (20 to 25%), quartz (13 to 15%), and minor metamorphic lithic components and other minerals (~2 %). The main sedimentary structure is fine horizontal and inclined parallel lamination (Figs. DR2 and DR4). Grain-size distribution curves from this unit are similar to the active dunes in the lowland, and differ from the present-day marine and Pleistocene curves (Fig. DR1).

A well-exposed section of these deposits exists at Punta Cochinos, the southern point of the island (section on Fig. DR2; aerial view on Fig. 4B). This section consists of a 0.5-m-thick dark-brown paleosol at the base, directly above the Tertiary rocks, which has a radiocarbon age of 31.5 ± 1.8 cka. It is overlain by four 1- to 4-m-thick beds of very well sorted brown sandstones with a rhythmic succession of horizontal and laminations dipping 30°E, interbedded with an undated, 0.5-m-thick paleosol in the upper part of the section.

Bioturbation is common in these sandstones. At Cadenas Peninsula we found well-preserved in situ trace fossils, which are exposed along a distinct horizontal depositional surface. The traces are cavities, composed of a 15-cm-long horizontal cylindrical part that bends upward into a 3-cm-high vertical section with a small circular opening (Fig. DR4). These features appear to be insect burrows. Kaizuka et al. (1973) described similar features in fixed Pleistocene dunes on Arauco Peninsula. These authors reported identical cavities filled with remnants of insects that belong to the family of tiger beetles (*Cicindelidae*), which are restricted to dry sandy environments (Pearson, 1988).

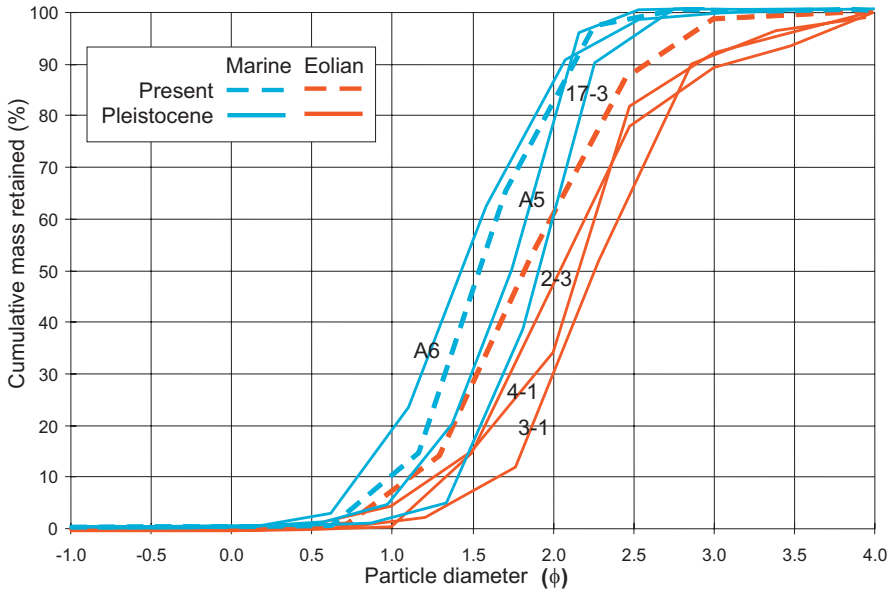

Figure DR1. Grain-size distribution curves comparing present and Pleistocene marine and eolian sands. The present marine samples is from the wash zone in the beach east of Puerto Sur. The present-day eolian sample is from the windward side of active dunes in the lowlands east of Puerto Norte. The Pleistocene marine samples are from the southern domain (A6 and A5) and from the northern domain (17-3). The Pleistocene eolian samples are from the northern (4-1 and 3-1) and southern (2-3) domains. Detail descriptions and extended data set in Jara (2006).

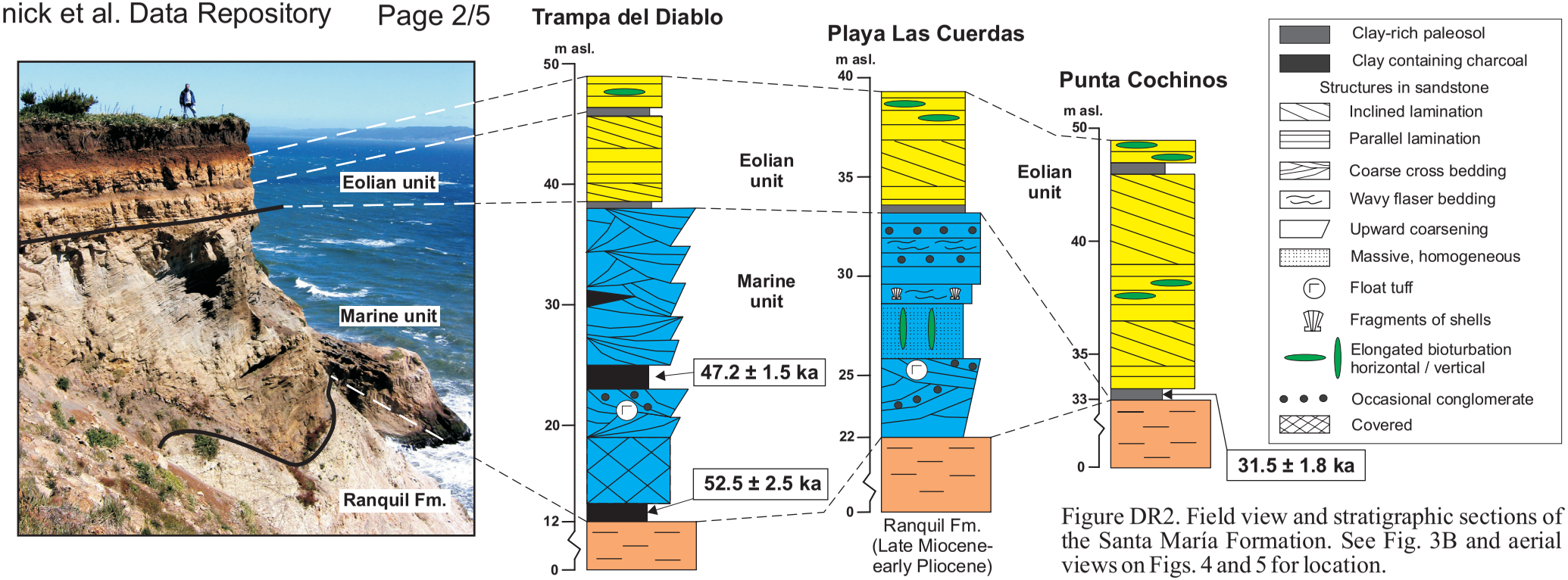

Figure DR2. Field view and stratigraphic sections of the Santa María Formation. See Fig. 3B and aerial views on Figs. 4 and 5 for location.

Figure DR3. View of shore facies of the marine unit north of Cadenas Peninsula. See Fig. 3A for location. Note the rhythmic interbedding between black sandstones, dark-brown paleosols (indicated with radiocarbon ages), and white to grayish layers of clay.

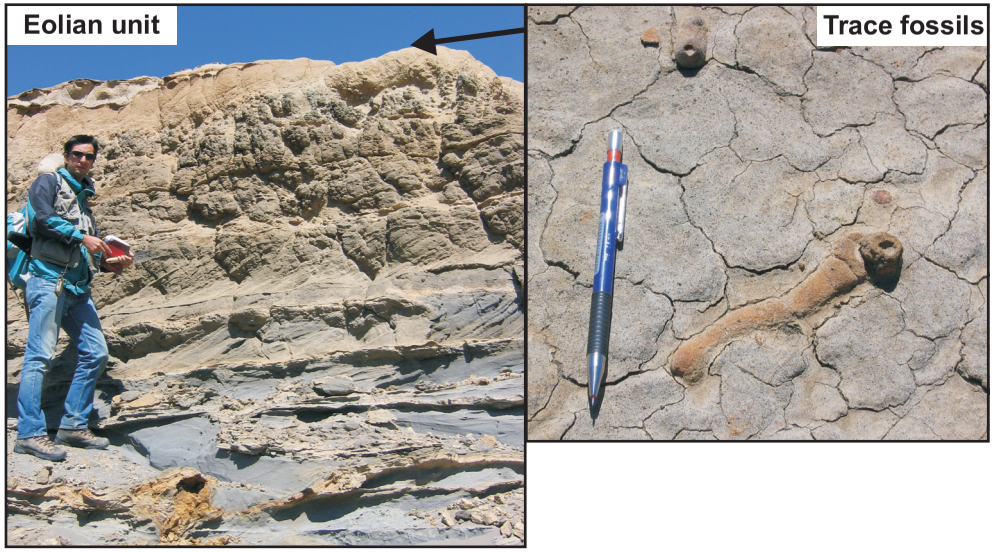

Figure DR4. View of the eolian unit at Cadenas Peninsula. Note the rhythmic succession of sandstone with inclined and horizontal lamination. Detailed view of trace fossils above the surface of the eolianite. These cavities are interpreted as insect burrows produced by tiger beetles, which presently live in dry sandy environments.

FACIES IN INCISED CHANNELS SURROUNDING CADENAS PENINSULA

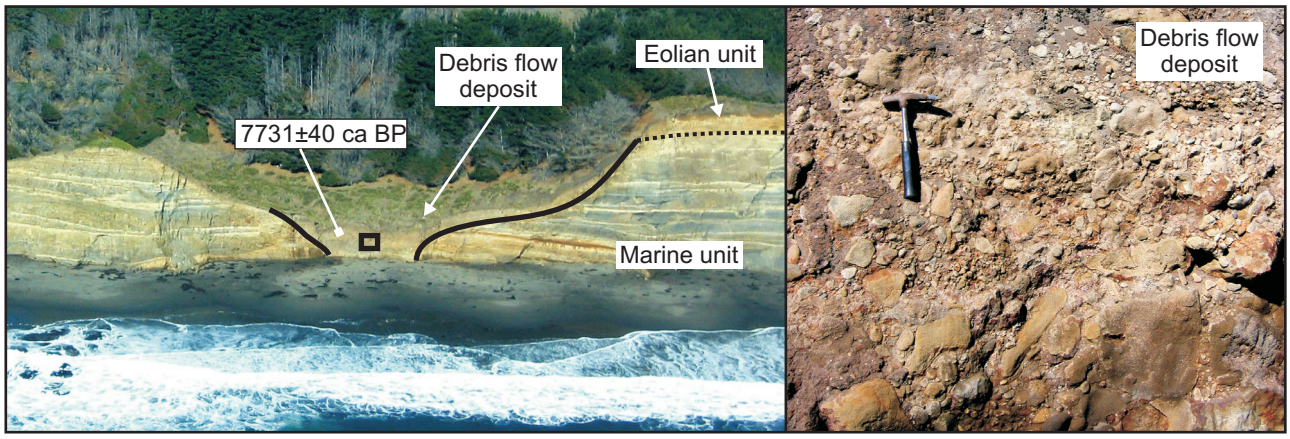

Figure DR5. Aerial view of an erosive channel incised in the Santa María Formation immediately north of the Cadenas Peninsula. See Fig. 3A for location. The stream was subsequently filled by a massive debris flow deposit. Radiocarbon age indicated in the deposit. The square shows location of detailed view on the right. The debris flow deposit is monomict, formed by angular brownish clasts from the Pleistocene eolian unit. The matrix is sandy with occasional lenses of fine material containing charcoal . Similar deposits crop out south of Cadenas Peninsula (see photo in Figure DR7-A; map on Figure 3A).

NORMAL FAULTING AND MARINE GROWTH STRATA

Northern Fault

The northern fault is well expressed at the western coast (Fig. DR6). The main fault dips 80°N and offsets the Tertiary/Pleistocene unconformity by 2.6 m; at 15 m distance from this structure, an antithetic normal fault dips 75°S and offsets the unconformity by 1.4 m. Both faults delimit a southward-tilted block of the Pleistocene sequence. The dip of the Pleistocene beds in the hanging wall decreases progressively upward indicating syntectonic sedimentation caused by slip on the north dipping growth fault (Fig. DR6). The tilted block is offset by a recent 0.4-m-slip rupture, which may have occurred during one of the past great earthquakes (Fig. DR6). The fault trace is very well preserved, and only limited material from the rupture zone has been removed by erosion. Farther west, this fault controls the only deep valley in the northern sector of the island (Fig. 3). The southern flank of this valley has steep slopes and the Tertiary/Pleistocene unconformity crops out continuously at ~10 m elevation The northern flank has lower slopes formed by gently-dipping Pleistocene beds in the backlimb of the tilted block, and the Tertiary/Pleistocene unconformity crops out at 5 m elevation.

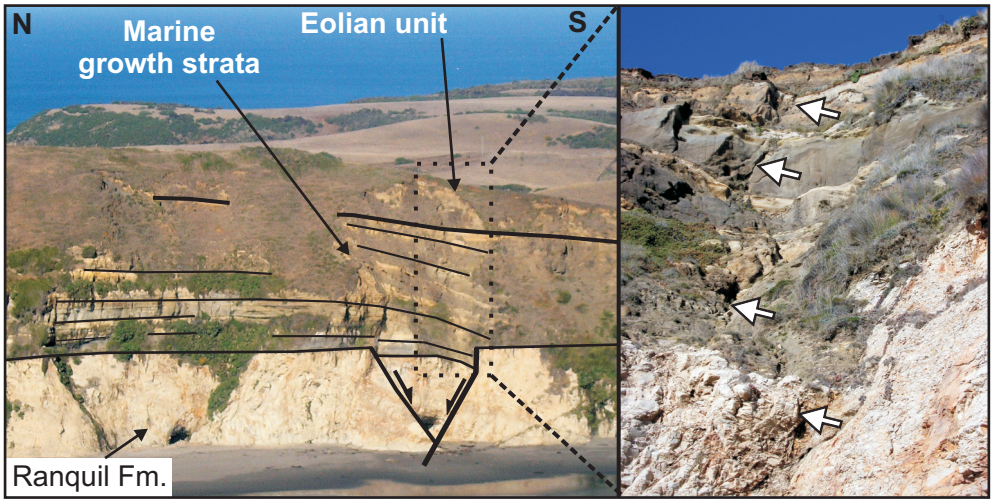

Figure DR6. Oblique air photo to the east showing the northern normal fault. Note progressive upward decrease in dip of the marine unit in the hanging wall of the north dipping fault. Detail field view of a recent rupture that produced a normal offset of 0.4 m.

Central Fault System

The depression and promontory in the center of the island are controlled by several faults that form a half-graben. This fault system divides the island into the two distinct tilt domains (Fig. DR7). This system includes: (1) a northwest dipping master fault south of the depression (Fig. DR7-B); (2) normal faults that form a horst-and-graben structure (Fig. DR7-A); (3) zones of intense fracturing and synsedimentary faulting of the Pleistocene marine sandstone; and (4) an intra-Pleistocene onlap surface (Fig. DR7-C). The profile shown in Figure DR7-D illustrates the geometry of the central half-graben. The main fault has a 30-cm-wide cataclastic zone and juxtaposes Tertiary siltstone and the Pleistocene Santa María Formation, with intense antithetic faulting in the hanging wall (Fig. DR7-B). This fault does not cut the upper unit. At Cadenas Peninsula, the marine unit is formed by two lithologically identical parts separated by an onlap surface; the horizontal upper beds onlap against similar underlying layers, which dip 30°SE (Fig. DR7-C). We relate the tilting of the lower beds to slip on the master growth fault and the onlap surface to progressive syntectonic sedimentation.

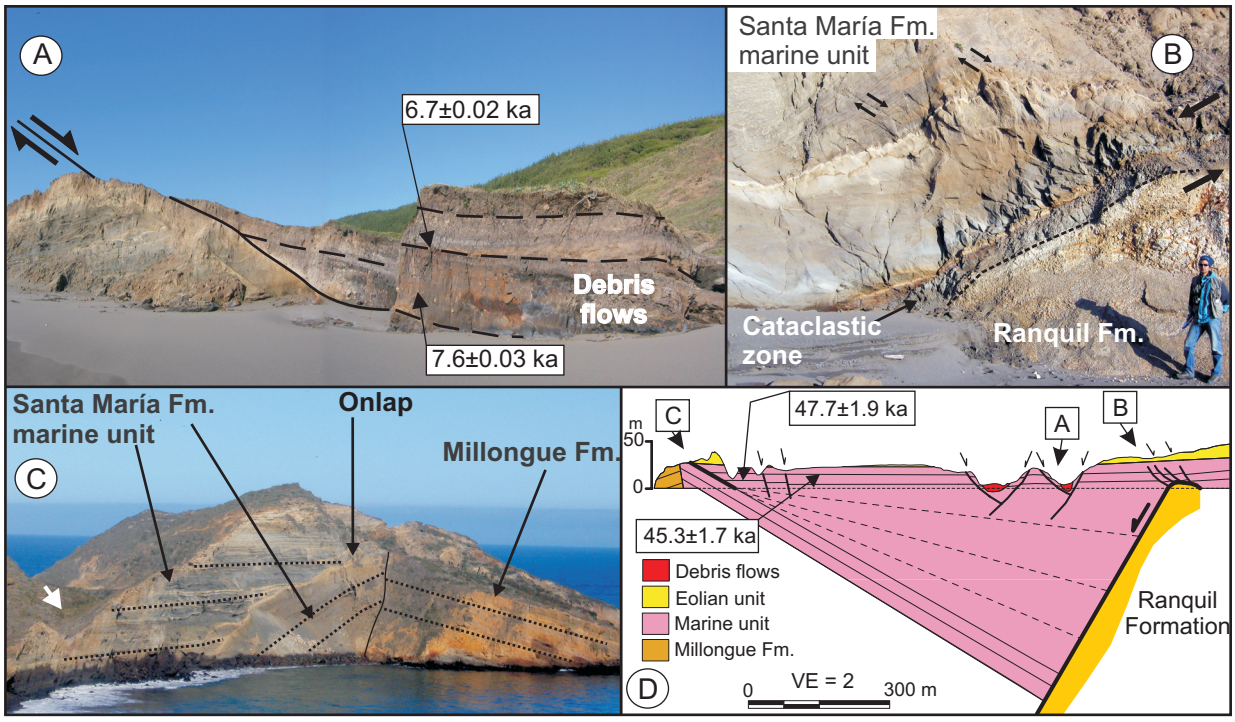

Figure DR7. Structures in the central part of the island. A: View of a normal fault and debris flow deposits with peaty matrix in the hanging wall with location of ^{14}C calibrated ages. B: View of the growth fault that juxtaposes Tertiary siltstone with Pleistocene marine sandstone. C: View toward the southwest of the Cadenas Peninsula showing the onlap surface within the marine unit of the Santa María Formation. D: Cross-section of the half-graben, location of calibrated ^{14}C ages, and interpretation of marine growth strata. Letters in squares show location of the photos.

Southern Fault

The southern fault strikes east-northeast and dips north; it is located at the southernmost point of the island and juxtaposes Tertiary rocks with the Pleistocene marine unit, which is absent in the footwall (Fig. DR8). The coastal marine sandstone in the hanging wall contain flame structures, injection veins, and are highly contorted, which we interpret as fault-related liquefaction features. Their distribution, as well as the intense vertical fracturation of the sandstone decreases steadily northward, away from the fault. The Tertiary rocks in the footwall are back-tilted 10°S and crop out 160 m north of the fault dipping 30°S (Fig. DR8). A 1.2-m-thick paleosol dips 30°S also above the Tertiary siltstone of the Ranquil Formation and the inclination of the overlaying marine sequence decreases continuously upward. We thus interpret the southern fault as a growth structure that controlled the syntectonic deposition of the Pleistocene marine sediments in the hanging wall.

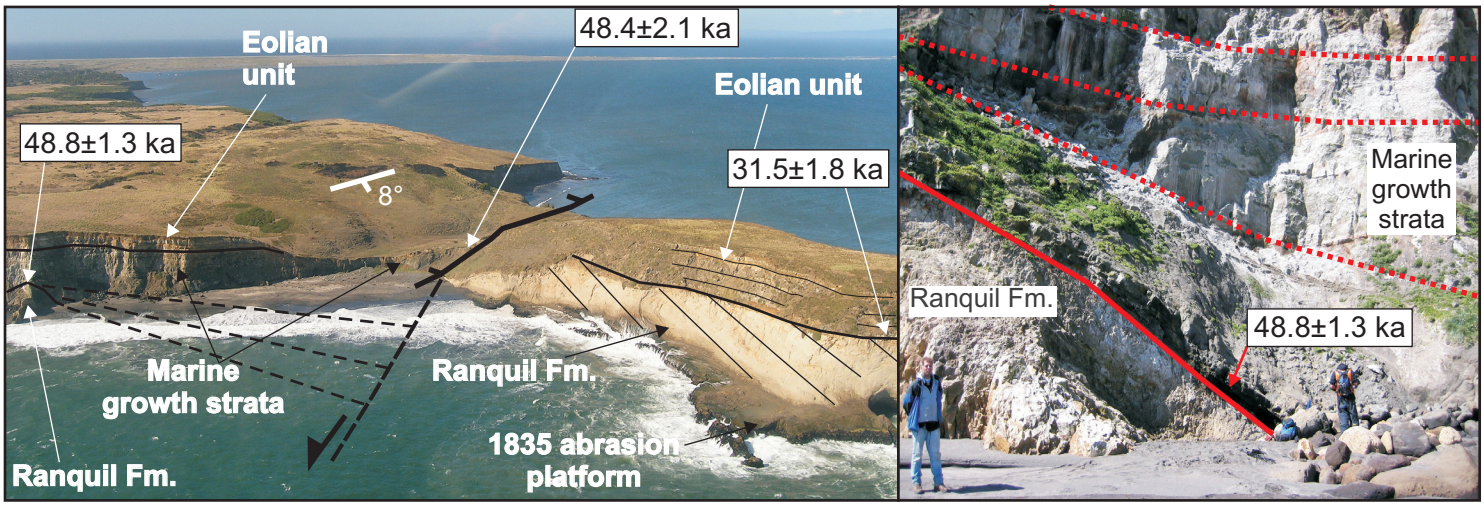

Figure DR8. Oblique air photo to the east and interpretation of the growth fault at the southern point of the island indicating calibrated ^{14}C ages. Note the back-tilting of the Ranquil Fm. in the footwall and absence of the marine unit. Contortion, intense vertical fracturation and liquefaction structures in the marine unit increase continuously toward the fault. The abrasion platform emerged during the 1835 earthquake can be seen in the lower right. Right: Marine sandstone dipping 30°S above Ranquil Fm. in the hanging wall of the fault. Note the upward decrease in dip of the sandstone sequence. Paleosol with calibrated ^{14}C age at the base of the marine unit.

TILTING RATES CALCULATION PROCEDURE

We used three reference surfaces to calculate the tilting rates of Isla Santa María: (1) the Tertiary/Pleistocene unconformity that is equal to the base of the marine unit and for which we assume a 51.6 ± 2.9 ka age (average of three ages); (2) the base of the eolian unit for which we assume a 31.5 ± 1.8 ka age; and (3) the present surface of the island for which we infer an age of 27 ± 2 ka based on sea-level data (see text). We believe that these erosional/depositional surfaces were subhorizontal at the time of their abandonment and that the subsequent tilting is only due to tectonic deformation. The well-preserved trace fossils found on the top of the eolian unit imply that erosion of this depositional surface is limited to the fluvial system.

In order to calculate realistic tilting angles, we measured the elevation of the three reference surfaces across eight profiles perpendicular to the tilt axis of the northern and southern domains (Fig. DR9). We judge our ability in measuring the elevations of the reference surfaces to be within ± 0.5 m. We derived four profiles for each tilt domain. The strike of the tilt axes was determined from the isobase contours of the Tertiary/Pleistocene unconformity, thickness variations of both units of the Santa María Formation, and the present topography analyzed from the high-resolution DEM (Fig. DR9). The elevation data, tilt angles and rates, and propagated errors of the three surface along the eight profiles are presented in Table DR1. The average values for each reference surface of both domains, together with their standard deviation and sum of errors is given in Table DR2.

	Northern Domain				Southern Domain			
Profile	**1**	**2**	**3**	**4**	**5**	**6**	**7**	**8**
Base marine unit								
Elevation West (m)	23.1	20.8	26.5	28.1	48.1	53.0	42.0	20.0
Elevation East (m)	10.1	16.8	3.2	4.0	<0	<0	9.8	4.2
Profile length (m)	250	266	1577	1476	2465	2451	1751	890
Tilt angle (degrees)	2.977	0.862	0.846	0.935	1.118	1.239	1.054	1.017
Tilting rate (°/ka)	0.058	0.017	0.016	0.018	>0.022	>0.024	0.020	0.020
Tilting rate error	0.008	0.005	0.002	0.002	>0.002	>0.002	0.002	0.003
Base eolian unit								
Elevation West (m)	25.9	40.0	31.0	32.0	57.0	53.0	45.0	35.0
Elevation East (m)	17.0	30.5	8.5	9.2	21.5	22.7	14.2	22.2
Profile length (m)	216	232	1546	1439	2432	2340	1690	829
Tilt angle (degrees)	2.359	2.345	0.834	0.908	0.836	0.742	1.044	0.885
Tilt rate (°/ka)	0.075	0.074	0.026	0.029	0.027	0.024	0.033	0.028
Tilt rate error	0.013	0.013	0.003	0.003	0.002	0.002	0.003	0.004
Present surface								
Elevation West (m)	57.0	57.0	57.0	60.0	68.0	55.0	52.0	36.0
Elevation East (m)	55.0	51.0	47.0	45.0	29.0	28.0	28.0	30.0
Profile length (m)	136	190	1419	1329	2357	2246	1515	796
Tilt angle (degrees)	0.843	1.809	0.404	0.647	0.948	0.689	0.908	0.432
Tilt rate (°/ka)	0.031	0.067	0.015	0.024	0.035	0.026	0.034	0.016
Tilt rate error	0.019	0.017	0.003	0.004	0.004	0.003	0.004	0.004

Table DR1. Field data and tilt rates calculated for three reference surfaces along eight profiles, four in each tilt domain (Figure DR9). For the calculation we assumed ages of 51.6 ± 2.9, 31.5 ± 1.8, and 27 ± 2 ka BP for the base of the marine unit, base of the eolian unit, and present-day surface, respectively, and ± 0.5 m error in the elevation measurements. Note that in profiles 5 and 6, the base of the marine unit is below sea level and hence we can only calculate a minimum rate.

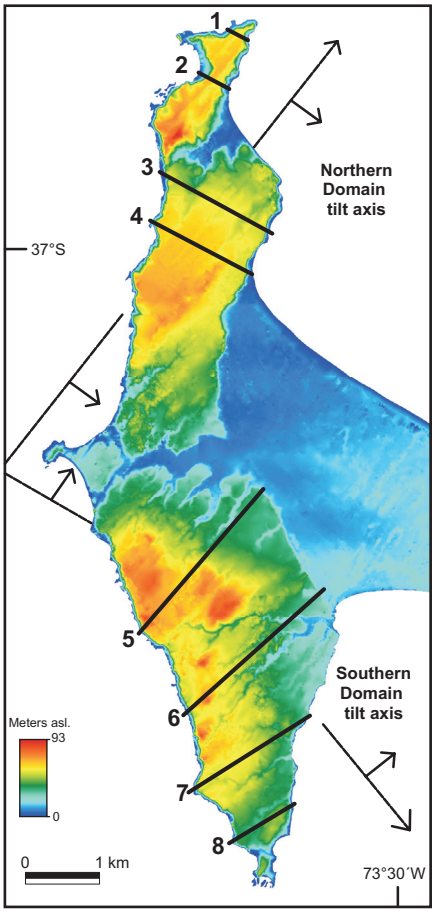

Figure DR9. DEM showing location of profiles used to calculate tilting rates.

Average tilt rates (°/ka)	Base Marine	1σ SD	Σ errors	Base Eolian	1σ SD	Σ errors	Present Surface	1σ SD	Σ errors	Average	1σ SD	Σ errors
Southern Domain	**0.021**	0.002	0.010	**0.028**	0.004	0.006	**0.028**	0.009	0.008	**0.026**	0.006	0.014
Northern Domain	**0.027**	0.020	0.004	**0.051**	0.027	0.019	**0.034**	0.023	0.026	**0.038**	0.024	0.033
Entire Island	**0.024**	0.014	0.011	**0.039**	0.022	0.020	**0.031**	0.016	0.028	**0.032**	0.018	0.036

Table DR2. Average tilt rates, standard deviation, and sum of errors for the three reference surfaces of each domain and the entire island.

Data Repository References

Jara, J., 2006, Análisis del alzamiento tectónico en Isla Santa María, evidencias sedimentológicas y geomorfológicas [Analysis of tectonic uplift at Isla Santa María, sedimentological and geomorphological evidences] [master thesis]: Universidad de Concepción, 110 p.

Kaizuka, S., Matsuda, T., Nogami, M., and Yonekura, N., 1973, Quaternary tectonic and recent seismic crustal movements in the Arauco Peninsula and its environs, Central Chile: Geographical Reports Tokyo Metropolitan University, v. 8, p. 1-49.

Pearson, D. L., 1988, Biology of Tiger Beetles: Annual Review of Entomology, v. 33, p. 123-147.

Vergara, M., and Katsui, Y., 1969, Contribución a la geología y petrología del volcán Antuco, Cordillera de los Andes, Chile Central: Departamento de Geología, Universidad de Chile, Publicación 35, p. 25-47.